Geometrical Optics of Dense Aerosols: Forming Dense Plasma Slabs

Michael J. Hay,[1,*] Ernest J. Valeo,[2] and Nathaniel J. Fisch[1,2]

[1]*Department of Astrophysical Sciences, Princeton University, Princeton, New Jersey 08544, USA*
[2]*Princeton Plasma Physics Laboratory, Princeton, New Jersey 08543, USA*

Assembling a freestanding, sharp-edged slab of homogeneous material that is much denser than gas, but much more rarefied than a solid, is an outstanding technological challenge. The solution may lie in focusing a dense aerosol to assume this geometry. However, whereas the geometrical optics of dilute aerosols is a well-developed field, the dense aerosol limit is mostly unexplored. Yet controlling the geometrical optics of dense aerosols is necessary in preparing such a material slab. Focusing dense aerosols is shown here to be possible, but the finite particle density reduces the effective Stokes number of the flow, a critical result for controlled focusing.

　　　　　　　PACS numbers: 82.70.Rr, 42.15.−i, 52.50.Dg

Introduction.—Certain applications in plasma physics require a dense plasma slab, but preparing an appropriately dense, shaped, and homogeneous plasma *in vacuo* is difficult. Rapidly ionizing a very dense aerosol jet offers a promising path to such a plasma, but the physics of focusing dense aerosols is entirely unexplored. In contrast, focusing effects in dilute aerosols have been the subject of extensive and fascinating work [1,2]. Focusing of dilute aerosols occurs through the formation of particle caustics as the flow passes through simple plate orifices, in analogy with geometrical optics. In the dense aerosol regime, this picture is modified by the coupling of the particulate and continuous phases. Although this coupling has been investigated in other contexts, the focusing of highly loaded flows is apparently unexplored. This Letter addresses such flows, uncovering new phenomena unique to the dense aerosol regime.

Dense aerosol regime.—To describe these phenomena, we envision a two-stage device (Fig. 1) that assembles a dense jet of particulate from a dilute, homogeneous suspension. We specialize to a rectangular lens geometry with slit lenses and aerosol sheets. Passing through the first stage, the aerosol is focused into a narrow jet. Although the gas Mach number at the focusing nozzle is small enough that the gas compressibility is unimportant, the spherical aerosol particles themselves are highly supersonic with respect to their Brownian motion: immense compression is possible [1]. In order to prepare high-density plasma targets, the aerosol phase will necessarily carry mass comparable to the carrier gas even prior to focusing. The second stage is a supersonic nozzle that greatly accelerates and expands the gas while imparting a small divergence angle and axial velocity kick to the aerosol sheet. Because the gas expansion is 2D, the gas density becomes negligible compared to the aerosol beam density downstream of the nozzle throat. Thus a steadily flowing, bare aerosol sheet is formed. The sheet can be ionized downstream of the nozzle by an intense laser pulse that produces the shaped, dense plasma.

In the dilute limit, focusing requires Stokes number $S \equiv \tau_d u_o / L_o \simeq 1$, where L_o is the size of the subsonic orifice, u_o is the gas flow speed there, and $\tau_d \equiv (2\rho_0 a^2 / 9\mu)(C_s / f_d)$ is a particle's velocity relaxation time due to drag on the carrier gas [2]. ρ_0 is the bulk density of the particle material, a the particle radius, μ the fluid viscosity, and $C_s \equiv 1 + (\lambda/a)[A_1 + A_2 \exp(-A_3 a/\lambda)]$ is the Cunningham correction for particle slip ($\lambda \propto 1/\rho_g$ is the gas-gas mean free path and the A_i's are order unity constants). $f_d \sim \mathcal{O}(1)$ corrects for finite particle Reynolds number. Additionally, unless the Reynolds number $\text{Re} \equiv \rho_g u_o L_o / \mu \lesssim 10^3$, the resulting turbulent flow is expected to disrupt the deterministic particle trajectories and inhibit focusing.

The supersonic nozzle orifice must be larger than the aerosol beam as focused by the subsonic nozzle upstream. Because ANSYS FLUENT simulations indicate $L_o / L_a \lesssim 10$ at $S = 1$, $L_o / L_n \lesssim 10$. Assuming an ideal gas equation of state for the carrier fluid and quasi-1D flow upstream of the supersonic nozzle throat, the Mach number in the central region must then exceed approximately 0.01 in order for $M = 1$ flow at the throat. Operating at sufficiently large Knudsen number $\text{Kn} \equiv \lambda/a \propto M/\text{Re}$ subsumes the Reynolds and Mach constraints. In the $\text{Kn} \gg 1$ regime,
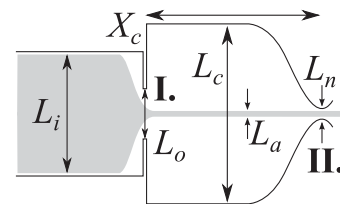

FIG. 1.　Schematic of two-stage system for compressing and extracting aerosol targets (gray). Stage I forms a jet from the isotropic suspension at the inlet. Stage II extracts this jet by dispersing the carrier gas. $\rho_{a,i}$ refers to the mean aerosol density upstream of stage I, ρ_a is the density between stages, and ρ_t is the final target density downstream of stage II.

$$S \simeq 0.70\sqrt{\gamma}\,\frac{a\rho_0}{L_o\rho_g}\,M_o, \tag{1}$$

where $M_o = u_o/c_g$ is the subsonic orifice Mach number, γ is the gas' adiabatic index, and $\mu = \bar{u}\lambda\rho_g/3$, c_g and $\bar{u}$ being the gas' sound and thermal speeds, respectively.

Together, these constraints on S, Re, and Kn impose an upper limit on the carrier gas density. The desired plasma electron density n_e determines the mean mass density of the spheres, $\rho_a \approx n_e(A/Z)M_p$, with A and Z denoting the aerosol material's mass and atomic numbers, respectively, and M_p the proton mass. Therefore,

$$\frac{\rho_a}{\rho_g} \gtrsim \frac{L_o}{1\text{ cm}}\sqrt{\frac{1\ \mu\text{m}}{a}\cdot\frac{1\text{ g/cm}^3}{\rho_0}}\left(\frac{n_e}{10^{19}/\text{cm}^3}\right). \tag{2}$$

In a homogeneous target ($n_a^{-1/3}/L_a < 10^{-2}$) suitable for compression of micron light, each factor will be $\mathcal{O}(1)$.

Aerodynamic focusing.—Several features of aerodynamic focusing were clarified by finite-volume FLUENT calculations. In the dilute regime, focusing was found to depend on only two parameters, S and Re. Passing through a simple slit orifice, calculations indicated that the contraction of the aerosol beam L_a/L_o exhibited a Re$^{-1/4}$ dependence with $S = 1$ fixed.

Operating at finite ρ_a/ρ_g introduces aberrations that together result in shifting optimal focusing to larger S as compared with a dilute flow of identical particles. Figure 2(a) shows $S \approx 0.9$ particles focusing tightly in the upper half of the channel. The velocity field and particle tracks have been calculated by FLUENT in the dilute limit, $\rho_{a,i}/\rho_g \equiv \rho_p/\rho \approx 0.001$. Apart from a single trajectory, carrying little density, there is very little widening of the envelope of particle trajectories downstream of the orifice. Figure 2(b) traces particles with τ_d identical to those in Fig. 2(a), albeit with significant momentum coupling between the continuous and discrete phases. Mass

loading lowers the orifice flow velocity and alters the gas streamline curvature, in turn reducing the "true" S as compared to Fig. 2(a)—we are using the flow parameters from otherwise equivalent simulations of dilute aerosol flows to estimate S in the dense cases. Hence, both S and τ_d are constant between Figs. 2(a) and 2(b) although the orifice velocity changes. The energetic aerosol particles subsequently increase the axial carrier velocity above the dilute calculation downstream of the orifice, resulting in small-divergence trajectories within $100L_o$.

Comparing Fig. 2(b) to Fig. 2(c), it is evident that increasing S at high mass loadings can reduce the sheet's divergence in the region immediately downstream of the orifice. In both cases, the relatively dilute edge of the beam has the greatest divergence angle due to drag on the carrier flow filling the channel. Figure 2(d) traces the larger S particles' paths in the dilute limit, confirming that adjusting S is responsible for the change in dynamics. At finite S, the beam tends to a negligible divergence far downstream due to the underlying Poiseuille flow.

Coagulation.—A severe operating constraint on the two-stage device is particle coagulation, which occurs upon a collision or approach within a distance characteristic of the van der Waals force. Upstream of the first stage, coagulation can destroy focusing and contribute to particle loss by altering the distribution of particle sizes. Downstream, where the residence time is very long and the particle density is large, coagulation reduces the homogeneity of the jet. The constraint pushes the operating regime to larger a, smaller L_a, and lower ρ_a.

Achieving homogeneity at high focused densities motivates operation in a regime where the effective scattering length l_B of an aerosol particle's Brownian motion is large compared to a: $l_B \equiv v_{th}\tau_d \gtrsim a$, where $v_{th} \simeq \sqrt{k_B T_g/m_p}$. T_g is the ambient carrier gas temperature and m_p is the mass of an aerosol particle. This results in a longer collision time due to Knudsen flow in a layer of radial extent l_B
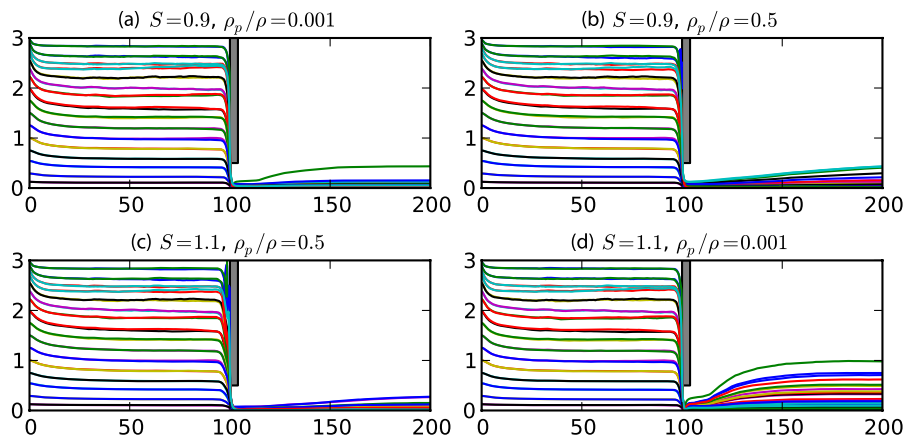

FIG. 2 (color online).   Representative particle tracks demonstrating aerodynamic focusing in four combinations of S and upstream $\rho_p/\rho = \rho_{a,i}/\rho_g$. In each frame (a)–(d), the abscissa is the horizontal displacement in multiples of L_o, the ordinate is the vertical displacement. The axial extent of the orifice is exaggerated for clarity.

surrounding each aerosol particle [3]. Most particle collisions occur between the two stages, so the constraint is determined there: $\tau_{\text{transit}}/\tau_{\text{coag}} \simeq (X_c/u_c)/\tau_{\text{coag}} < 1$. u_c is the axial gas speed in the central region and $\tau_{\text{coag}} \simeq (2\sqrt{2}\pi n_a a^2 v_{th}\delta)^{-1}$, where $n_a \equiv \rho_a/m_p$ is the number density of spheres [3]. $\delta \leq 1$ is the fraction of collisions resulting in coagulation. Note the strong dependence on particle size: $\tau_{\text{coag}} \propto a^{5/2}$ at fixed ρ_a. The need to avoid coagulation thus establishes a minimum particle size, above which beam divergence due to Brownian motion is also negligible.

Target density and aspect ratio.—We assume fluid descriptions for the coupled gas and aerosol flows in order to calculate the focused target's density and divergence. Although the particle Knudsen number is large, the criterion for continuum flow is easily satisfied: $\lambda/L_o \ll 1$. Because the particle volume fraction $\rho_a/\rho_0 \ll 1$, the body force coupling the two fluids is $\propto \rho_a(\mathbf{u}_a - \mathbf{u}_g)/\tau_d$. Within the focused aerosol beam, $\rho_a/\rho_g \gg 1$, so we may neglect inertia in the gas momentum equation to obtain

$$\mathbf{u}_g \simeq \mathbf{u}_a - \frac{\tau_d}{\rho_a}\nabla p_g. \tag{3}$$

Assuming an equation of state $p_g = p_g(\rho_g)$, the gas continuity equation has the convection-diffusion form:

$$\frac{\partial \rho_g}{\partial t} + \nabla \cdot \rho_g \mathbf{u}_a = \nabla \cdot \frac{\tau_d}{\rho_a}\rho_g c_g^2 \nabla \rho_g, \tag{4}$$

where $c_g^2 = \partial p_g/\partial \rho_g$. Near the subsonic orifice, the aerosol compression of order L_i/L_o can drive a corresponding $\Delta\rho_g$. In steady state, the gas diffusion compensates the convective aerosol compression:

$$\rho_g \frac{\hat{\mathbf{y}} \cdot \mathbf{u}_a}{L_o} \sim \frac{\tau_d \rho_g c_g^2}{\rho_a L_o^2}\Delta\rho_g, \tag{5}$$

where $\hat{\mathbf{y}}$ is the transverse flow direction. Then

$$\frac{\Delta\rho_g}{\rho_g} \sim \alpha \equiv \frac{2L_o^2}{\gamma a^2} \cdot \frac{\rho_a \rho_g}{\rho_0^2} \ll 1 \tag{6}$$

if we can neglect the carrier gas compressibility. This is a consistency condition for the two-fluid model: $\alpha < 1$ restricts particle trajectory crossings due to coherent hydrodynamic motion. If $\alpha \ll 1$, the radial diffusion of gas in the focused beam is faster than axial convection:

$$\nu_\perp \sim \frac{\tau_d \rho_g c_g^2}{\rho_a L_a^2} \gg \hat{\mathbf{x}} \cdot \mathbf{u}_a \frac{d}{dx}\log L_a \sim \nu_\parallel \tag{7}$$

and $\partial\rho_g/\partial y$ is accordingly negligible. Then $L_a \simeq$ const and the summed momentum equations for the two phases have a first integral:

$$\frac{S_a}{L_a}u_a + p_g(\rho_g) \equiv \text{const}, \tag{8}$$

where $S_a \equiv \rho_a u_{a,x} L_a \simeq$ const. If $M \gg 1$ downstream of the supersonic nozzle, $p_g \to 0$ and Eq. (8) implies that

$$u_{a,f} \lesssim \frac{L_a}{S_a}p_{g,i}, \tag{9}$$

where $u_{a,f}$ is the final downstream aerosol speed and $p_{g,i}$ is the gas pressure far upstream of the focusing device. The acceleration of the aerosol beam is limited by a "barreling" effect that depends on the contrast ratio ρ_a/ρ_g.

As $\rho_g(x)$ decreases through the supersonic nozzle, a transverse pressure gradient $\partial p_g/\partial y$ is established that can in turn develop a diverging $u_{a,y}$. Comparing the axial convection and radial diffusion terms of Eq. (4),

$$u_{a,x}\frac{\partial\rho_g}{\partial x} \sim \frac{\partial}{\partial y}\frac{\tau_d\rho_g c_g^2}{\rho_a}\frac{\partial\rho_g}{\partial y}, \tag{10}$$

and substituting the y component of the summed momentum equations,

$$\rho_a u_{a,x}\frac{\partial u_{a,y}}{\partial x} = -c_g^2\frac{\partial\rho_g}{\partial y}, \tag{11}$$

we estimate the divergence as

$$\frac{u_{a,y}}{u_{a,x}} \sim \frac{L_a/\tau_d}{u_{a,x}} \simeq \frac{L_a}{L_o}\alpha^{1/2}, \tag{12}$$

where we have estimated $\partial/\partial y \sim 1/L_a$ and $u_{a,x} \sim (\rho_g/\rho_a)^{1/2}v_{th}$ from Eq. (9). The maximum aerosol speed limits the extracted target density:

$$\frac{\rho_t}{\rho_{a,i}} \simeq \frac{L_i u_i}{L_a u_{a,f}} = \frac{L_o^4(\rho_a\rho_g)_i}{a^2 L_a^2 \rho_0^2} = \frac{L_o^2}{L_a^2}\alpha, \tag{13}$$

where $S = 1$ to eliminate the upstream gas velocity u_i.

The consistency criterion for the two-fluid model is $\alpha \ll 1$, but the final target density is small in this limit

TABLE I. Dense aerosol operating constraints.

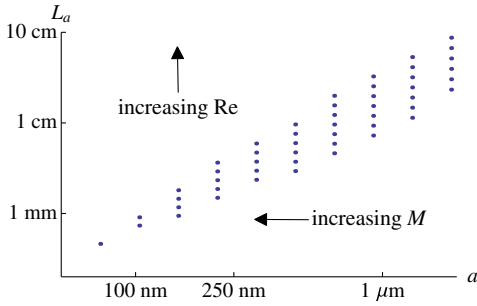|	
	$S = 1$
	$10 < \text{Re} < 500$
Stage I	$\alpha < 1$
	$M_o \equiv u_o/c_g < 0.3$
	$\text{Kn} \equiv \lambda/a > 1$; $\lambda/L_o < 1$
	$X_c > 10L_i$
	$L_c > L_a$
Between stages	$X_c/u_c < \tau_{\text{coag}}$
	$l_B/a > 1$
	$M_n = 1$
	$L_n > L_a$
Stage II	$\text{AR} \equiv (L_a\alpha^{1/2}/L_o)^{-1} > 10$
	$n_a^{-1/3}/L_a < 10^{-2}$
	$\rho_t \simeq 0.017(A/Z)(n_e/10^{19}/\text{cm}^3)\ \text{mg/cm}^3$

FIG. 3 (color online). Possible operating points at $n_e \simeq 10^{19}$ cm^{-3} and $\rho_0 = 2$ g/cm^3 in (a, L_a) space. Each point is parametric in Re and M; the labeled arrows indicate tendencies.

TABLE II. Accessible ρ_t for select materials. The maximum average mass density in the target was calculated for 100 nm $< a < 1$ μm and 1 mm $< L_a < 1$ cm using an optimization procedure constrained by the relations in Table I.

Material	ρ_0 (g/cc)	max ρ_t (mg/cc)
CH	1.0	0.10
Fe	7.9	2.7
Ni	8.9	3.2
W	19.2	5.1
Au	19.3	5.2

per Eq. (13). Per Eq. (12), the target aspect ratio scales as $\alpha^{-1/2}$; intermediate α is necessary for high-quality targets. It is more important to operate in a large L_o/L_a regime, which occurs for $S = 1$ and Re $\gtrsim 10^2$.

Operating points.—Table I lists these and other pertinent constraints. Considering $n_e \simeq 10^{19}$ cm^{-3} plasmas suitable for Raman compression, the available targets are charted in Fig. 3. To compress intense light and attain large geometric convergence, large aspect ratio geometries are necessary. We estimate AR $\gtrsim 10$ to be satisfactory, beyond what is available with gas jets. We note that 5-mm targets are available with good homogeneity: $a/L_a \sim 10^{-5}$. At fixed a, small-L_a targets below the boundary identified in Fig. 3 are too inhomogeneous. Likewise, L_a above the region in Fig. 3 require high M and high Re operation that could result in deleterious shocks, turbulence, etc. At fixed (a, L_a), a higher-density target is subject to those constraints; the (a, L_a) operating space tends to widen as ρ_t is reduced. Note that the particle trajectories between stages were assumed to have zero divergence before entering the second stage.

Alternative techniques and applications.—Alternative techniques for producing a plasma slab suffer from limitations that might be overcome using the dense aerosol approach. Aerogels and foams are characterized by filamentary structures. In laser plasmas, the time scales over which the filaments vaporize and the target material homogenizes must be much shorter than the time required for the rarefaction wave at the target edge to move a distance comparable to the initial target width. Because a typical filament has a large aspect ratio, it expands in 2D and such structures can persist late in the ionizing pulse [4,5]. Gas jets lack a solid matrix but are instead saddled with short hydrodynamic time scales associated with turbulent eddies and the propagation of shocks from the nozzle.

Fast Raman compression in plasma couplers may enable the next generation of laser intensities [6]. Although first-generation experiments use capillary-shaped plasmas a few millimeters in length and transverse sizes of about 50 μm [7], ionized dense aerosols could be engineered to have the

same length but much larger transverse sizes to accommodate more power [8]. These pancake-shaped plasmas require good uniformity at electron densities greater than 10^{19} cm^{-3}, with transverse lengths of several centimeters.

Low-divergence aerosol targets could surpass the efficiencies of gas jets in radiator experiments on Z [9]. However, the homogeneity and aspect ratio requirements are relaxed somewhat compared to those required for Raman compression; here, a satisfactory design point is a 1-cm jet of 1-μm nickel particles, $\rho_0 = 8.9$ g/cm^3. Larger particles are less susceptible to coagulation; the Reynolds constraint (2) guarantees operation in a moderately dense aerosol regime: $\rho_a/\rho_g \gtrsim 10^2$ at $\rho_t \approx 1$ mg/cc. Table II summarizes the target densities achievable with polystyrene (CH) and a few metals.

Similar dense aerosol schemes could offer structured targets to the MagLIF program, which is expected to rely on laser heating of annular targets [10]. FLUENT calculations suggest that a focus with $S \gtrsim 1$ will have a radial density profile peaking on axis; further increasing S will result in an annular density profile. By choosing different S for each phase, a single lens can yield gradients in material composition with differential focusing, e.g., an annulus of one phase ($S > 1$) filled by another ($S \approx 1$).

Summary.—Self-consistent momentum coupling between aerosol and carrier flows changes the aerodynamic focusing properties of the system. The particle loading reduces the effective Stokes number in the first stage, shifting the focus; in the second stage, the aerosol is so dense that it dominates the flow field and the particles move ballistically.

The focusing properties of aerodynamic lenses permit the design of dense, homogeneous, high-aspect ratio targets. Jets of small spherical particles could be engineered to homogenize quickly with minimal turbulent features. Because so many solid and liquid species can be aerosolized, these targets open up the design space for plasma targets. Separating the target's assembly and ionization permits complex designs with tailored gradients that could improve current plasma technologies.

*hay@princeton.edu

[1] J. F. de la Mora and P. Riesco-Chueca, J. Fluid Mech. **195,** 1 (1988).

[2] P. Liu, P. J. Ziemann, D. B. Kittelson, and P. H. McMurry, Aerosol Sci. Technol. **22,** 293 (1995).

[3] N. A. Fuchs, *The Mechanics of Aerosols* (MacMillan, New York, 1964).

[4] A. E. Bugrov, S. Y. Gus'kov, V. B. Rozanov, I. N. Burdonskiĭ, V. V. Gavrilov, A. Y. Gol'tsov, E. V. Zhuzhukalo, N. G. Koval'skiĭ, M. I. Pergament, and V. M. Petryakov, J. Exp. Theor. Phys. **84,** 497 (1997).

[5] G. J. Caporaso, Phys. Fluids **25,** 436 (1982).

[6] V. M. Malkin, G. Shvets, and N. J. Fisch, Phys. Rev. Lett. **82,** 4448 (1999).

[7] Y. Ping, W. Cheng, S. Suckewer, D. S. Clark, and N. J. Fisch, Phys. Rev. Lett. **92,** 175007 (2004).

[8] Z. Toroker, V. M. Malkin, A. A. Balakin, G. M. Fraiman, and N. J. Fisch, Phys. Plasmas **19,** 083110 (2012).

[9] H. Sze, J. Banister, B. H. Failor, J. S. Levine, N. Qi, A. L. Velikovich, J. Davis, D. Lojewski, and P. Sincerny, Phys. Rev. Lett. **95,** 105001 (2005).

[10] S. A. Slutz and R. A. Vesey, Phys. Rev. Lett. **108,** 025003 (2012).